Research Square

Preprints are preliminary reports that have not undergone peer review.
They should not be considered conclusive, used to inform clinical practice,
or referenced by the media as validated information.

Ghost rivers beneath cities: a major blind spot of flood-risk governance

Celso Garcia

celso.garcia@uib.es

University of the Balearic Islands https://orcid.org/0000-0002-4584-9732

Jorge Lorenzo-Lacruz

University of La Rioja

Ramon Batalla

University of Lleida

Enrique Morán-Tejeda

University of the Balearic Islands

Aaron Ortega-Mclear

University of the Baleairc Islands

Sònia Vives Sònia Vives

University of the Balearic Islands

Article

Keywords:

Posted Date: November 3rd, 2026

DOI: https://doi.org/10.21203/rs.3.rs-11082904/v1

License: This work is licensed under a Creative Commons Attribution 4.0 International License.
Read Full License

Additional Declarations: There is **NO** Competing Interest.

Ghost rivers beneath cities: a major blind spot of flood-risk governance

Celso Garcia[1], Jorge Lorenzo-Lacruz[2], Ramon J. Batalla[3], Enrique Morán-Tejeda[1], Aaron Ortega-Mclear[1], Sònia Vives[4]

1. Department of Geography. University of the Balearic Islands, Palma, Spain
2. Department of Human Sciences, University of La Rioja, Logroño, Spain
3. Fluvial Dynamics Research Group RIUS, University of Lleida, Catalonia, Spain
4. Centre d'Estudis de Postgrau, University of the Balearic Islands, Palma, Spain

Abstract

As cities expand over floodplains, the streams crossing them are occasionally buried; yet these ghost rivers keep their hydrological function, generating runoff and flash floods that endanger the populations above. For the first time, we located and inventoried 50 ghost rivers entombed during twentieth-century urbanisation of Spain's Mediterranean coast, a climate-change and tourism hotspot repeatedly struck by catastrophic floods. Three-quarters of these streams lie beneath coastal cities and resorts; the remainder beneath intensive agriculture. Most (64%) fall outside the official flood-risk register, an exclusion that does not track physical hazard (catchment morphometry and soil sealing). Moreover, the unrecognised catchments receive more, not less, extreme rainfall. This registration pattern instead reflects the social geography of the coast: among 377,625 residents of these catchments, the poorer are captured in the map while the wealthier remain administratively invisible. This structural blind spot in urban flood governance has potential implications far beyond the Mediterranean.

As cities expand, rivers are often buried beneath urban development. The covering, culverting and channelling of urban streams is among the most pervasive yet least visible transformations of the urban landscape: streams that once threaded through valleys and coastal plains now run unseen beneath streets, car parks and buildings[1-6]. The ecological costs of this transformation, the so-called urban stream syndrome[7,8], are well documented, and a daylighting movement in the cities of North America, northern Europe and East Asia has sought to reverse it[9–12]. But the great majority of buried urban streams remain hidden, surviving only as conduits beneath the contemporary city. Urbanisation therefore creates a fundamental contradiction: rivers remain active hydrological systems while progressively disappearing from the institutional frameworks through which flood risk is recognised and governed.

This contradiction is becoming increasingly apparent as climate change intensifies flood hazards in densely urbanised regions. Although ghost rivers are buried in their lower reaches, their upstream catchments continue to receive precipitation and to concentrate runoff, now routed across

an urban surface and through a drainage network never designed to carry it. The Mediterranean is an illustrative example of this dynamic, where high-intensity convective storms meet some of the most densely urbanised coastlines in Europe: the catastrophic flash floods of the DANA of October 2024[13], which claimed almost 240 lives in the metropolitan periphery of Valencia, showed how water routed across obliterated channels can overwhelm the modern city. Flash floods on the Mediterranean coast are closely linked to convective rainfall[14], and under high-emission scenarios the intensity of daily rainfall extremes is projected to increase over much of the northern Mediterranean, even where annual precipitation declines[15,16]. Because stream burial itself accelerates the storm response of urban catchments and makes flooding sensitive to failures of subsurface infrastructure[17], these hidden channels are likely to become an increasingly important component of urban flood risk for the populations living above them.

Contemporary flood-risk governance depends on institutional recognition. Flood hazards can only be governed once they have been identified, mapped and incorporated into the administrative frameworks that underpin spatial planning, emergency management and environmental regulation. In the European Union, the Floods Directive (2007/60/EC) obligates member states to map flood hazard and to align land-use planning, emergency response and development control accordingly[18]; in Spain this is implemented through the National System of Flood Zone Cartography (SNCZI) and the associated register of areas of potential significant flood risk (APSFR). This framework rests on a prior act of recognition: a watercourse must first appear in official hydrographic inventories. A stream erased from the urban surface, often from civic memory, and then from those inventories becomes invisible to every instrument designed to govern its hazard, a condition we term *administrative invisibility*: the disappearance of physically active rivers from the institutional frameworks through which flood risk is recognised and governed. Although urban stream burial has been studied as an ecological and geomorphological problem[19,20], and urban flooding as a hazard[21], little attention has been paid to how burial reshapes the governance of flood risk.

Here we assemble the first regional inventory of ghost rivers, streams buried during the twentieth-century expansion of Mediterranean Spanish cities and coastal resorts. Specifically, we ask: (i) Where are ghost rivers located and which urban areas do they underlie? (ii) Does their exclusion from official flood-risk cartography reflect genuine differences in hydrological hazard, or is it a consequence of administrative invisibility? (iii) How is this institutional disconnection socially distributed across urban populations?

A regional inventory of buried urban streams

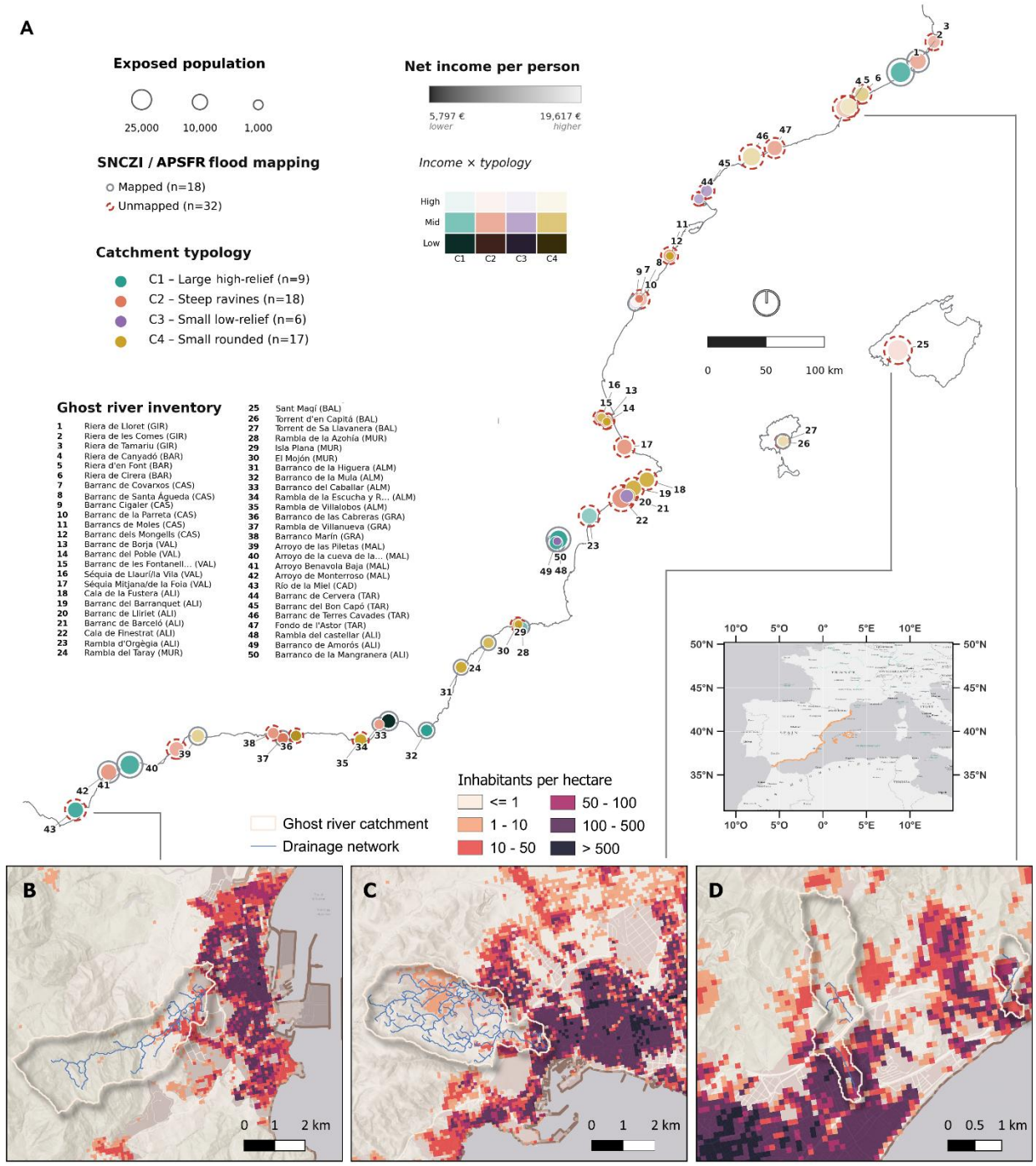


Fig. 1. (A) Location and inventory of the 50 ghost-river catchments along the Spanish Mediterranean coast and the Balearic Islands. Marker fill combines catchment typology (hue) with median net income per person (shade; darker = lower income); marker area is proportional to exposed population; rings denote official flood-risk recognition (solid grey, APSFR-mapped, n = 18; dashed red, unmapped, n = 32). Numbers correspond to the ghost-river inventory, in which the three-letter codes in parentheses denote the Spanish province in which each ghost river lies (ALI, Alicante; ALM, Almería; BAL, Illes Balears; BAR, Barcelona; CAD, Cádiz; CAS, Castellón; GIR, Girona; GRA, Granada; MAL, Málaga; MUR, Murcia; TAR, Tarragona; VAL, Valencia); (B) detailed view of the ghost-river catchment at

Algeciras (Andalusia; 123,435 inhabitants) and distribution of exposed population; (C) as in (B), for Palma (Balearic Islands; 424,837 inhabitants); (D) as in (B), for Badalona (Catalonia; 221,750 inhabitants).

The identified streams concentrate in the coastal cities and tourist municipalities that grew most intensely after 1960[22], with the highest densities along the coasts of Catalonia (13), Alicante (12), Almería (8) and Málaga (5), a pattern that shows ghost rivers to be not isolated anomalies but a widespread legacy of twentieth-century Mediterranean urbanisation, embedded within the urban fabric of rapidly expanding coastal cities. Two mechanisms account for the disappearance of these channels. Urban burial dominates (37 cases; 74%): channels culverted, paved over or absorbed into the stormwater networks of cities such as Badalona, Benidorm, Palma and Algeciras (Fig. 1). Agricultural burial (13; 26%) comprises channels obliterated by intensive agriculture, primarily the greenhouses of the Campo de Dalías (Almería) and the irrigated plains of Castellón, Valencia and Alicante. The agricultural cases also sit within the same coastal-development frontier, frequently discharging towards downstream settlements.

Catchment areas span from 0.07 to 21.32 km² (median 2.30 km²; skew 1.57), so the inventory is dominated by small basins alongside a few larger systems. Mean slope ranges from 0.7% to 50.6% (median 22.9%) and relief from 3 m to 795 m (median 297 m), reflecting the steep coastal fronts where distances from summits to the shore are short (Extended Data Fig. 1). Planforms are markedly elongated to moderately compact (circularity 0.12–0.47, median 0.27), characteristic of catchments that generate peaked, fast-rising hydrographs.

A Spearman's rank correlation matrix performed over catchments morphological metrics (Extended Data Fig. 2) shows two largely independent blocks: a *size block* (area, perimeter and Strahler order; pairwise ρ=0.89–0.98, $p < 0.001$) and a *relief block* (mean slope, maximum slope, relief and mean elevation; relief–slope ρ=0.64). Area and mean slope are uncorrelated (ρ=0.15, p=0.30), indicating that small urban catchments are not inherently gentler than large ones.

Four typologies of ghost-river catchments

Ward clustering applied to the 50 ghost-river catchments, based on seven standardised morphometric variables yielded four catchment typologies (Fig. 2; Table 1), visualised by a principal component analysis whose first two axes captured 71.6% of the variance (Fig. 2B). The four types are: C1, large high-relief catchments (n = 9), rising in coastal ranges and engulfed downstream by urban or agricultural growth; C2, steep ravines (n = 18), of moderate size but the steepest and most compact of the inventory, a combination that favours rapid runoff concentration; C3, small low-relief basins (n = 6), draining gentle coastal plains and fans; and C4, small rounded catchments (n = 17), the most numerous group and the archetypal buried city stream.

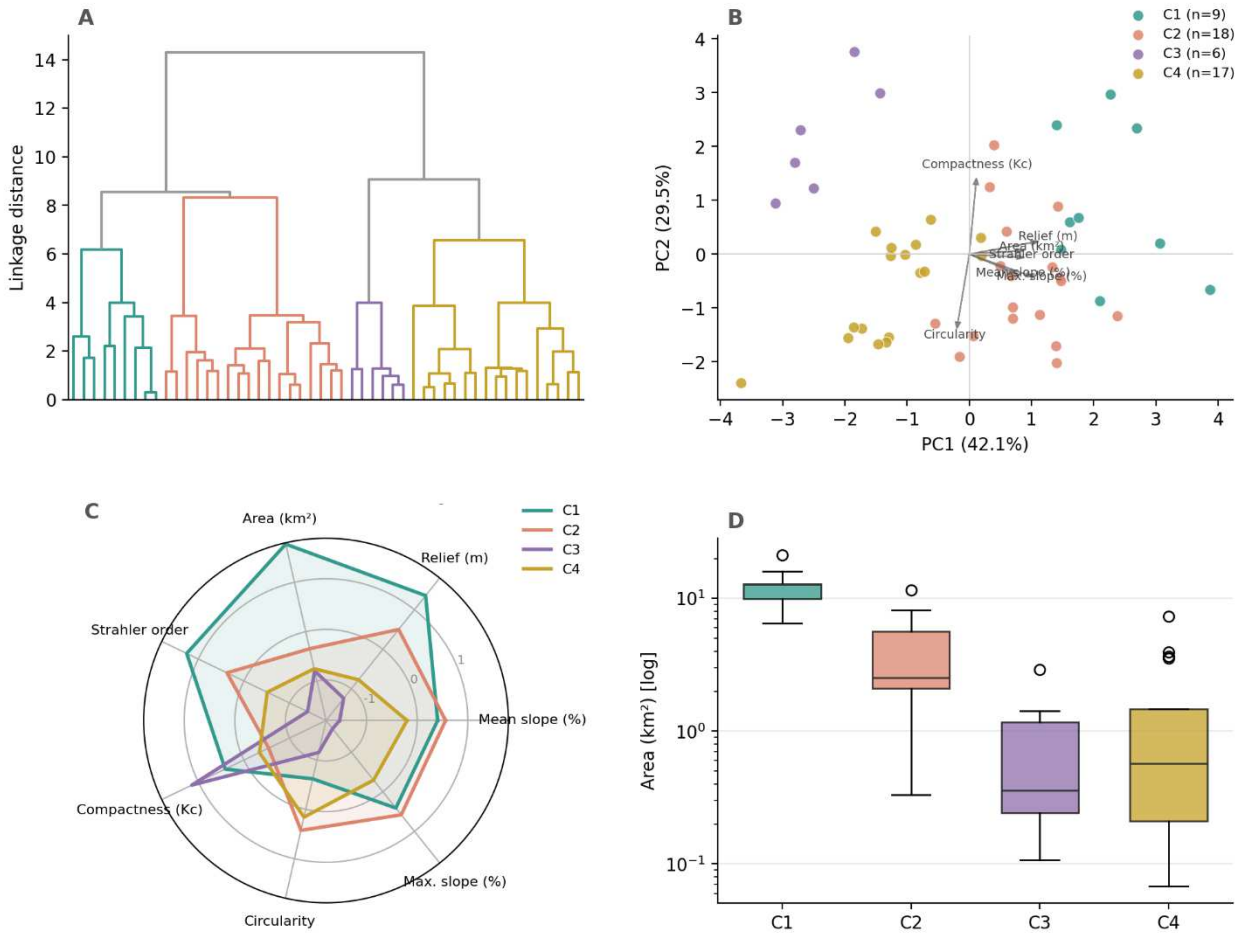


Fig. 2. Catchment typology from Ward clustering (k = 4, n = 50): (A) Ward dendrogram; (B) principal component biplot with cluster membership and variable loadings (PC1 42.1%, PC2 29.5%); (C) standardised median radar profiles by cluster; (D) catchment area by cluster (log scale; boxes, interquartile range; centre line, median; whiskers, 1.5× IQR; points, outliers).

Additionally, Mann–Whitney U tests revealed no statistically significant morphometric differences between urban (n = 37) and agricultural (n = 13) ghost-river catchments in six of the seven variables tested (Extended Data Table 1; Extended Data Fig. 3). Urban catchments tend to be larger (median 2.55 vs. 1.38 km²), steeper (mean slope 24.1% vs. 12.8%; $p = 0.070$) and of higher channel order ($p = 0.069$), but only maximum slope differs significantly (median 80.6% vs. 56.0%; $p = 0.002$). Apart from this contrast, the absence of systematic morphometric differences suggests that ghost rivers are defined by processes of land transformation rather than by distinctive physical characteristics.

Table 1. Morphometric profiles of the four ghost-river typologies (median values).

Variable	C1 (n=9)	C2 (n=18)	C3 (n=6)	C4 (n=17)
Area (km²)	12.71	2.52	0.36	0.57
Relief (m)	597	421	61	158
Mean slope (%)	26.2	28.0	3.8	19.2
Max. slope (%)	87.1	93.3	14.5	61.5
Circularity	0.221	0.300	0.181	0.280
Compactness (Kc)	2.13	1.83	2.36	1.89
Strahler order	3	2	0	1
Urban / Agric.	7 / 2	15 / 3	3 / 3	12 / 5

Flood-risk recognition and hydrological hazard

Of the 50 catchments, only 18 (36%) fall within an APSFR designated under the SNCZI; the remaining 32 (64%) lie entirely outside the official flood-risk register. Intersection with the with the SNCZI's modelled inundation envelopes (T_{50}, T_{100} and T_{500}) shows that 25 catchments (50%) intersect at least one extent, while the other 25 intersect none. Where an overlap exists it is small: a median of 2.34% of catchment area at T_{100} and 3.43% at T_{500}, reflecting envelopes largely confined to the channel corridor (Extended Data Table 2).

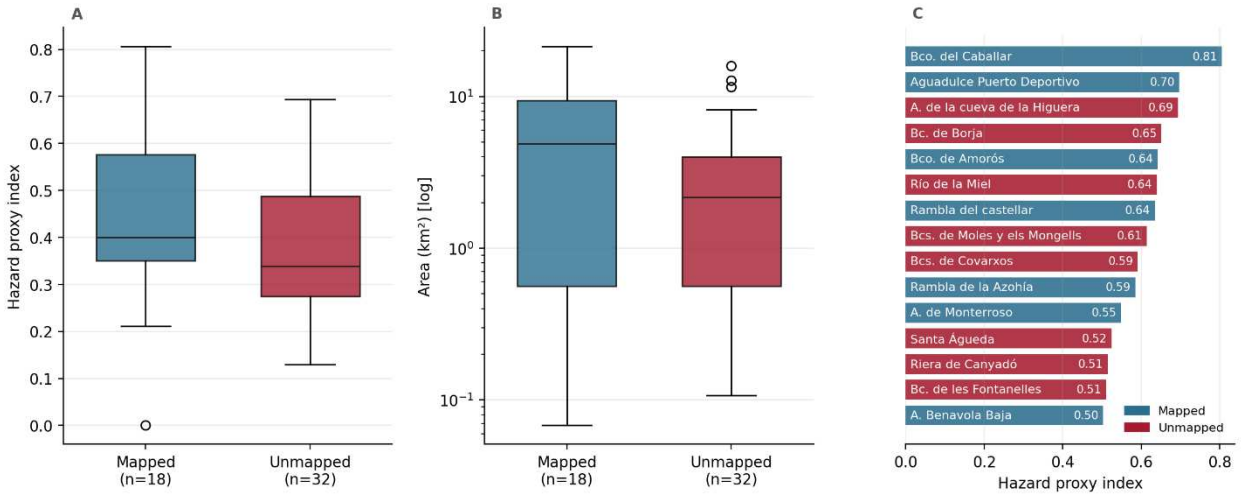


Fig. 3. Flood-risk recognition versus morphometric hazard (n = 50): (A) composite morphometric hazard proxy by APSFR status (centre line, median; two-sided Mann–Whitney U test P = 0.084); (B) catchment area by APSFR status (log scale); (C) the fifteen highest-hazard catchments, with bars coloured by APSFR status (mapped vs. unmapped).

The absence of official recognition cannot be explained by lower hydrological hazard. A Mann–Whitney U test between catchments inside and outside the APSFR register reveals no significant difference in any morphometric variable (all $p > 0.19$; Extended Data Table 3). The composite

morphometric hazard proxy, combining normalised mean slope (0.4), relief (0.3) and compactness (0.3), does not differ significantly either (Fig. 3A; median 0.400 vs. 0.339; $p = 0.084$). Mapped and unmapped catchments overlap on the attributes that should matter most: their hazard distributions (Fig. 3A) and drainage areas (Fig. 3B) are broadly similar, and the two groups sit interleaved along the full hazard ranking rather than sorting into high- and low-risk ends (Fig. 3C). The recognition boundary is therefore not explained by intrinsic differences in catchment hazard. The one attribute that does separate the two groups is the modelled flood coverage itself (T_{500}: median 0.88% vs. 0%; p = 0.046), an unsurprising result: because an APSFR is delineated through a hydraulic study, a mapped flood extent is a precondition of designation rather than an independent attribute that could distinguish designated from non-designated streams. Recognition thus separates the catchments that have been hydraulically studied from those that have not, rather than the hazardous from the non-hazardous. This disconnection provides empirical support for the concept of *administrative invisibility*.

A screening with the Spanish standard rational method (Témez; Instrucción 5.2-IC) confirms that this similarity extends to hydrological hazard: for the 100-year design storm, unmapped catchments generate peak discharges comparable to recognised ones (median 33.2 vs. 36.5 m^3/s; $p = 0.86$) but significantly higher specific discharges (19.7 vs. 10.2 $m^3/s/km^2$; $p = 0.010$) and runoff coefficients (0.67 vs. 0.57; $p = 0.008$), with 27 of the 32 unmapped catchments exceeding the median specific discharge of the recognised ones (Extended Data Fig. 5). Their exclusion therefore corresponds to a persistent (and, per unit area, more torrential) flood hazard, not a lesser one.

A latitudinal gradient in extreme rainfall

Because the inventory spans almost six degrees of latitude, we examined whether climatic forcing varies systematically along the coast. For each catchment we obtained the 50-, 100- and 500-year quantiles of annual maximum daily precipitation (Methods). Extreme rainfall increases significantly northwards (Spearman $\rho = 0.40$, 0.38 and 0.36 for T_{50}, T_{100} and T_{500}; all $p < 0.01$), but the gradient is better described as a pronounced maximum in the central Valencian sector (39° N, see shaded latitude band in Fig. 4A): mean 500-year daily rainfall rises from 192 mm in the southern catchments (Cádiz to Murcia, n = 17) to 307 mm in the centre (Alicante to Castellón, n = 20), with maxima of 420–462 mm in streams 14 to 17 (Fig. 4A).

This climatic gradient is hydrologically consequential and statistically independent of the morphometric one. The 100-year return period daily precipitation shows a positive rank association with the modelled flooded fraction of the catchment at the same return period (Spearman $\rho = 0.43$, p = 0.034; Fig. 4B), consistent with climatic forcing contributing to the exposure pattern. Yet this rainfall is uncorrelated with the composite morphometric hazard proxy ($\rho = 0.04$) or with mean slope ($\rho = 0.19$; both $p > 0.18$), and it does not predict real soil sealing ($\rho = -0.16$), which is instead governed by catchment morphology (Fig. 4D). Climatic and

morphological hazard are therefore orthogonal dimensions, neither of which is captured by the official recognition criteria.

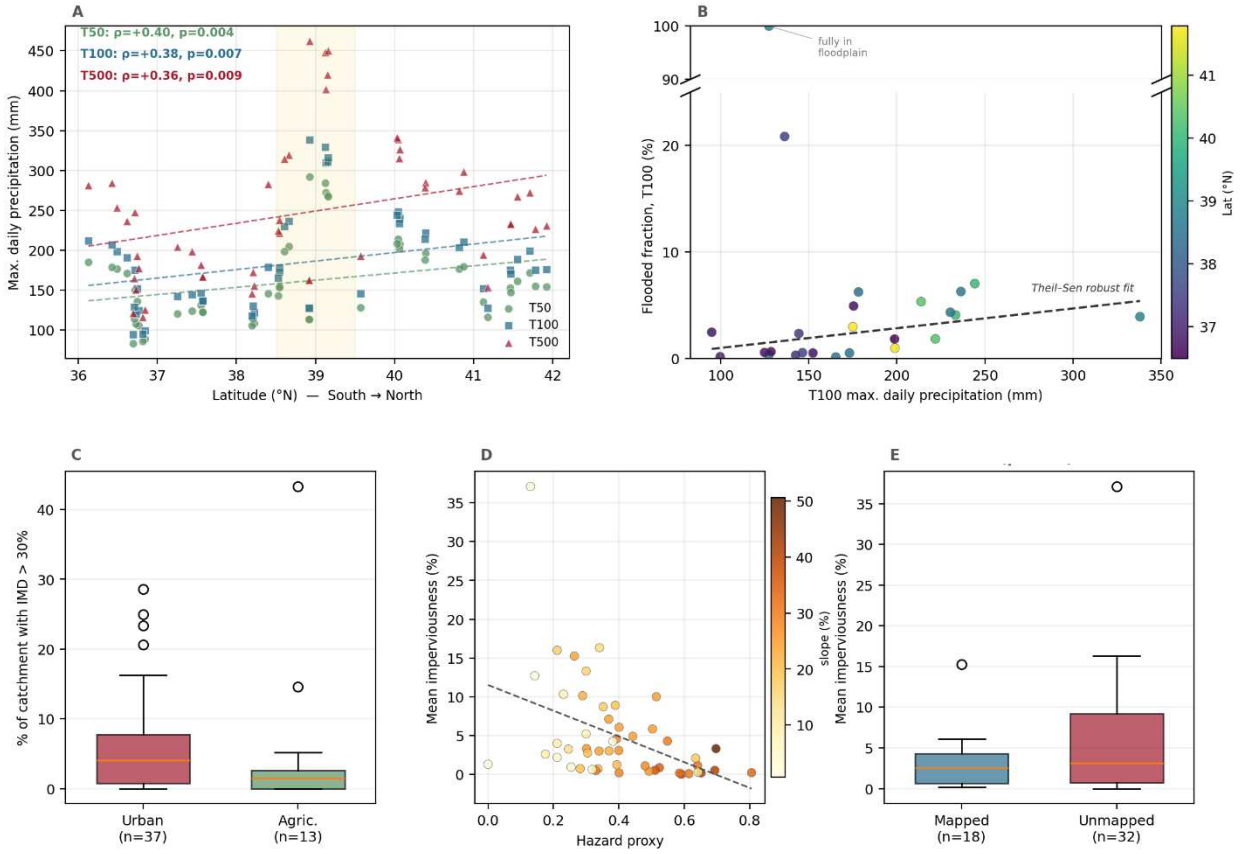


Fig. 4. Top (A,B), extreme precipitation (return-period quantiles of annual maximum daily precipitation; CSIC observational grid, ≈2.5 km): (A) 50-, 100- and 500-year daily precipitation versus latitude, with dashed linear fits and Spearman ρ and P for each return period (n = 50); the shaded band marks the central Valencian sector; (B) 100-year design rainfall versus the modelled flooded fraction of the catchment for the 25 catchments touched by a flood extent, coloured by latitude (broken y-axis; Spearman ρ = 0.43, P = 0.034). Bottom (C–E), real imperviousness (Copernicus Imperviousness Density 2021, 100 m): (C) percentage of catchment area exceeding 30% sealing in urban (n = 37) versus agricultural (n = 13) burial catchments (two-sided Mann–Whitney U test P = 0.071); (D) mean imperviousness versus the composite morphometric hazard proxy, coloured by mean slope, with a dashed linear fit (Spearman ρ = -0.49, P < 0.001); (E) mean imperviousness by flood-risk recognition status (APSFR), no significant difference (P = 0.41). Boxes, interquartile range and median; whiskers, 1.5× IQR.

Catchment imperviousness and the recognition gap

We quantified each catchment's degree of urbanisation with the 2021 Copernicus Imperviousness Density layer[23]. Soil sealing is low and is governed by morphology: it correlates negatively with the hazard proxy (Fig. 4D; ρ = -0.49, $p < 0.001$) and with mean slope (ρ = -0.46), indicating the contrast between rural steep headwater catchments and urbanised low-relief coastal basins. Urban-burial catchments are consequently more sealed than agricultural ones (median 4.1% vs. 1.5% of catchment area above 30% imperviousness; $p = 0.071$; Fig. 4C), a contrast that becomes

unambiguous among catchments smaller than 1 km² (median catchment mean imperviousness 8.0% vs. 2.2%). Imperviousness does not differ between mapped and unmapped catchments (Fig. 4E; median catchment mean 2.6% vs. 3.1%; $p = 0.41$). Official flood-risk recognition is therefore not associated with the degree of urbanisation either.

Populations exposed

To characterise the populations exposed, we intersected the 50 catchments with the 2021 census sections, assigning each section to the catchment with which it most overlapped, from which it inherited its flood-risk status (Methods). The catchments overlie 190 census sections across 12 provinces, home to 377,625 inhabitants, mostly urban neighbourhoods of coastal cities and resorts.

Table 2. Socioeconomic comparison between census sections in mapped (APSFR) and unmapped catchments (two-sided Mann–Whitney U test; n = 64 mapped and 126 unmapped, 190 sections).

Indicator	Mapped	Unmapped	P	Sig.
Annual net income/person (€)	10,885	12,720	<0.001	***
Annual net income/household (€)	27,849	33,035	<0.001	***
Income/consumption unit (€)	16,869	19,631	<0.001	***
Population ≥65 years (%)	16.7	19.0	0.009	**
Mean age (years)	42.0	43.7	<0.001	***
Sections < national avg.	85.9%	54.8%	—	—
Total population	135,408	242,217	—	—

Residents of officially mapped (APSFR) catchments are poorer: median net income per person is €10,885, against €12,720 in unmapped catchments (census sections, n = 64 vs. 126; Mann–Whitney $p < 0.001$; rank-biserial r = 0.46, 95% CI 0.31–0.61), and the difference is consistent across household income and income per consumption unit (Table 2; Fig. 5). Because sections are nested within catchments, we verified the contrast with a catchment-level permutation test ($p = 0.03$; cluster-bootstrap 95% CI for r 0.12–0.70). Weighted by population, the 135,408 residents of mapped catchments live in neighbourhoods with a median income of €10,891, against €12,556 for the 242,217 residents of unmapped ones; 86.8% versus 57.8% fall below the national average income (Supplementary Table 1). This gap is not a regional artefact: it is absent in the uniformly low-income south ($p = 0.32$) but widens within the wealthier central and northern coasts (€9,526 vs. €11,305, $p = 0.001$, in the centre and €11,882 vs. €15,006, $p < 0.001$, in the north), indicating that recognition tracks relative disadvantage within regions rather than absolute poverty (Fig. 5D). The populations of unmapped catchments, besides wealthier, are also modestly older (median share aged ≥65 of 19.0% vs. 16.7%, $p = 0.009$; mean age 43.7 vs. 42.0 years, $p < 0.001$). The eight

lowest-income catchments are predominantly mapped, headed by the catchment of stream 33 in Almería (€5,797 per person; Extended Data Table 4).

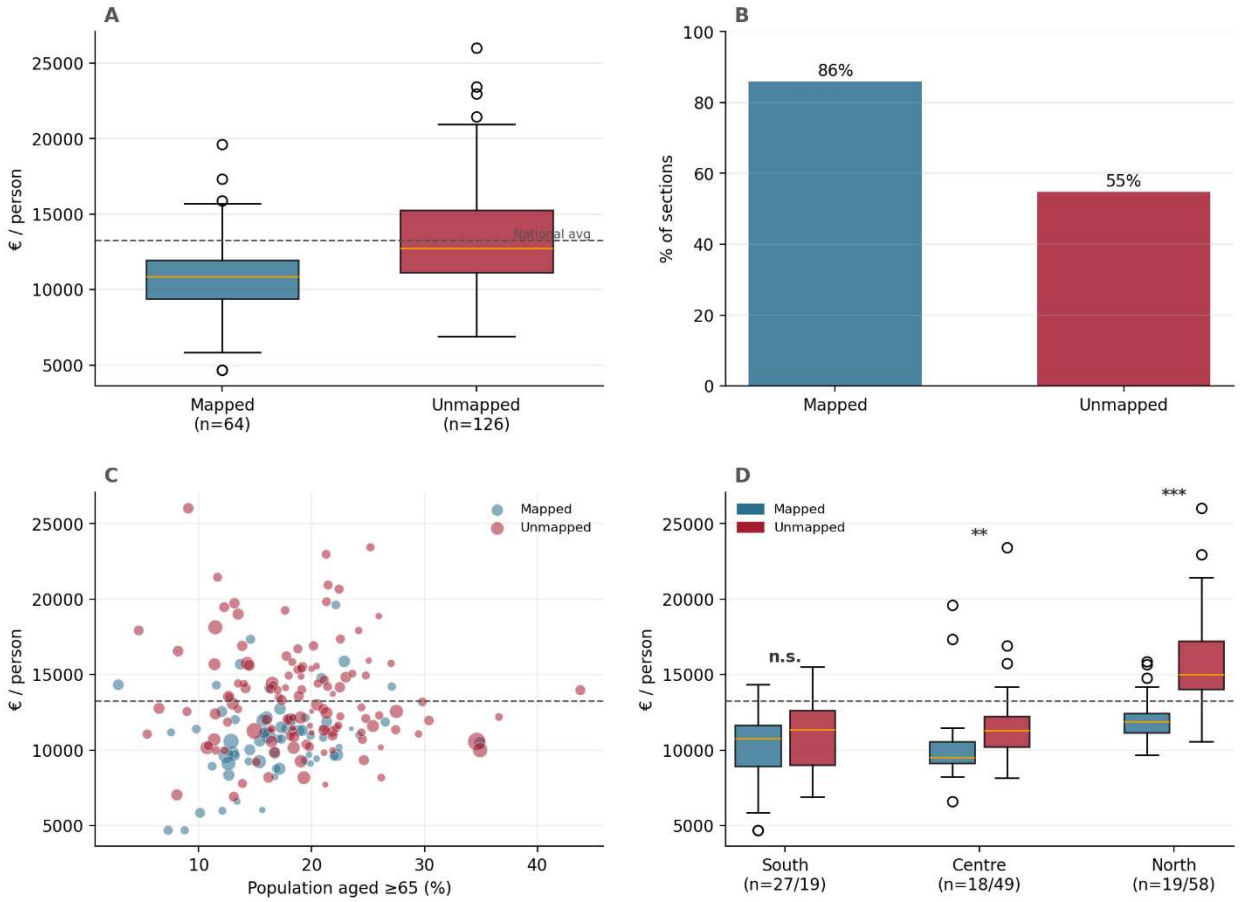


Fig. 5. (A) net income per person in census sections of recognised versus unrecognised catchments, with the national-average reference line (boxes, interquartile range; centre line, median; two-sided Mann–Whitney U test $P < 0.001$; n = 64 and 126 sections; catchment-level cluster permutation test $P = 0.03$); (B) percentage of sections below the national-average income; (C) section income versus the share of population aged 65 and over, with marker area proportional to section population; (D) net income per person by flood-recognition status within three coastal regions (South, Centre and North), showing that the income gap persists within regions (Mann–Whitney U test: not significant in the south, $P = 0.001$ in the centre, $P < 0.001$ in the north). Income data, ADRH 2021 (n = 190 sections).

Discussion

The identification of 50 ghost rivers provides the first systematic, representative and city-regional account of buried urban streams, whose culverted channels pose a persistent flood risk[11,24,25], and shows how stream burial can disconnect physically active hazards from the frameworks that govern urban flood risk. The ghost-river phenomenon is inseparable from the urbanisation that produced it: the concentration of ghost rivers along the segments of coast that urbanised most rapidly from the 1960s confirms that their origin lies in the specific model of tourism- and residential-led coastal city growth that prevailed in Mediterranean Spain, largely unregulated until

the 1985 Water Act and subsequent hydrological planning[26]. The dominance of urban over agricultural stream burial (74% vs. 26%) underscores that this is, first and foremost, a story about cities. More broadly, these findings contribute to debates on uneven geographical development[27]: urbanisation produces not only uneven urban landscapes, but also new forms of administrative invisibility and uneven flood-risk governance.

Despite their modest size (median area of 2.30 km²), these urban catchments possess the geomorphology to deliver rapid and dangerous hydrological response, i.e. steep gradients (median slope 22.9%), substantial relief and elongated planforms that favour peaked hydrographs[28,29]. The independence of size and slope is decisive for governance: the small catchments most easily dismissed as negligible are not systematically gentler than the large ones. Conventional channel-network descriptors would in any case understate the true hydrological connectivity of urbanised ghost rivers, whose natural networks have been replaced by impervious surfaces and channels that amplify rather than attenuate runoff[8]. The upstream suppression of first- and second-order channels, which in natural catchments delay and attenuate flood peaks, may further exacerbate downstream risk: the geomorphic changes that urban expansion imposes on these networks have been linked to a ten- to twenty-fold increase in bankfull flood discharges[30].

The four-catchment typology offers a template for differentiated urban management. The large high-relief catchments of Cluster 1, whose developed channels are comparable to mapped rivers, are prime candidates for hydraulic-corridor reservation or partial daylighting, strategies already realised in Mediterranean cities such as Barcelona (Besòs)[31] and Valencia (Turia)[32], and their omission from flood inventories is the least defensible. The steep streams of Cluster 2 demand attention to extremely short warning times within urbanised areas, while the numerous small streams of Clusters 3 and 4, individually minor but collectively pervasive, call for the systematic re-inclusion of buried channels in municipal drainage and emergency planning.

A cartographic gap in urban flood governance

The finding that 64% of ghost-river catchments lie outside the APSFR register, despite showing no significant morphometric difference from recognised (mapped) catchments (hazard proxy p = 0.084) and, if anything, a more torrential hydrological response, suggests a systematic gap in how urban flood risk is assessed and managed. Institutional recognition tracks income (rank-biserial r = 0.46) more strongly than the morphometric hazard proxy (r = 0.30), and the unmapped catchments receive more, not less, extreme rainfall. The SNCZI, like the EU Floods Directive it implements, recognises hazard only where a stream already exists in official inventories[33,34]; a stream erased from the urban surface and struck from those inventories falls outside every downstream instrument, from land-use restriction to municipal emergency planning and the environmental assessment of new development. *Administrative invisibility* is therefore distinct

from the 'hidden risk' of the hazards literature[35,36]: the hazard is not merely unperceived by residents but actively excluded from the frameworks through which authorities assess and manage it. The solution lies not only in improving risk communication but also in revising the criteria by which urban streams are incorporated into hydrological inventories.

Climate and urbanisation as independent hazard dimensions

Extreme rainfall increases northwards along the coast but peaks in the central Valencian sector, where the DANA storms responsible for the 2024 floods affected some of the most heavily buried catchments, and it is positively correlated with the modelled flooded fraction ($\rho = 0.43$). Administrative recognition, however, does not align with climatic exposure: recognised catchments receive significantly lower extreme rainfall than unrecognised ones (median 100-year rainfall: 143 vs. 184 mm; $p = 0.019$). Soil sealing is governed by morphology and does not differ between recognised and unrecognised catchments (2.6% vs. 3.1%; $p = 0.41$). Recognition thus follows neither morphometric hazard, climatic exposure nor the intensity of urbanisation, reinforcing the idea that administrative invisibility is institutional rather than environmental in origin.

An urban-environmental paradox

Recognition maps onto the poorer neighbourhoods (Table 2). Administrative invisibility is therefore not simply a concentration of hidden hazards in deprived areas: institutional recognition and social vulnerability follow different spatial logics, so that official flood-risk governance only partially overlaps with the geography of socioeconomic disadvantage[37,38].

Two limitations frame this socioeconomic reading. First, net income is only a partial proxy for social vulnerability, which also depends on housing tenure, age, gender, migration background and adaptive capacity[39] (dimensions our census-based analysis cannot fully resolve). Second, that recognition maps onto the poorer areas is not a claim that the wealthy are more vulnerable, but that administrative invisibility redistributes flood-risk exposure along a different axis than deprivation alone. The two groups face qualitatively distinct injustices: residents of recognised, poorer catchments bear a disproportionate share of officially acknowledged hazard, whereas residents of unrecognised, wealthier catchments face a hazard the institutional frameworks do not see, and against which the protections that recognition triggers are unavailable. Wealthier households may command private means of adaptation that partly offset this, though the governance failure is common to both. Administrative invisibility is therefore best understood as a failure of procedural justice (who and what enters those frameworks) that precedes and reshapes the distributive question of who is exposed[40].

Governing what cannot be seen

Administrative invisibility names a specific failure: not that a hazard is unknown, but that it is absent from the instruments that make hazards governable. It therefore sits between literatures that have so far run in parallel. Research on infrastructural invisibility has shown how buried networks recede from public and political attention until they fail[41] and the gradual and undramatic character of that erasure can be seen as a form of slow violence[42]. Additionally, studies of state legibility show that what an administration cannot see it cannot regulate[43]. Environmental justice scholarship has documented how flood risk concentrates along lines of social disadvantage[37,38], and the hazards literature has described risks attenuated in perception[36]. Ghost rivers bring these strands together: they represent a hazard that is physically active, socially forgotten and, decisively, institutionally unregistered, a failure of procedural rather than distributive justice[40].

Our inventory of 50 ghost rivers, though the most comprehensive to date, is not exhaustive; further buried streams surely persist beneath older urban settlements where all surface trace is lost. Nevertheless, a clear pattern emerges: in cities where urbanisation has buried streams, their absence from flood-risk cartography appears to stem from their omission from official hydrographic inventories, rather than from evidence that they represent a lower level of flood hazard. These streams drain the neighbourhoods of 377,625 residents, and the cartographic blind spot falls on specific urban populations rather than on hydrologically marginal terrain. Ghost rivers are not simply buried streams, but evidence of a structural form of administrative invisibility. In this sense, ghost rivers reveal uneven geographical development expressed through the unequal institutional recognition of environmental hazards.

Methods

Inventory and catchment delineation. Ghost rivers were identified along the Spanish Mediterranean coast by combining historical cartography, multi-temporal orthophotography and field survey to locate streams present in pre-development records but absent or buried in the contemporary urban fabric or agricultural surface. For each, the point of disappearance (burial point) was geolocated and the contributing catchment delineated from the 5-m PNOA digital terrain model (https://centrodedescargas.cnig.es; sink filling, D8 flow direction[44] and accumulation, snapping of the burial point to the modelled channel, and watershed extraction) in QGIS and SAGA[45], in ETRS89/UTM (EPSG:25830–25831).

Burial classification. Each catchment was assigned to urban or agricultural burial by interpretation of the disappearance mechanism (culverting, paving and stormwater integration versus land levelling and greenhouse construction).

Morphometric analysis. All indices were computed uniformly across the inventory from area, perimeter, channel-network elevations, slope and Strahler order[46]. Shape was described by the

circularity ratio ($Rc = 4\pi A/P^2$) and the Gravelius compactness coefficient ($Kc = P/2\sqrt{(\pi A)}$); relief as the elevation range (Extended Data Table 5).

Clustering. Seven standardised variables (area, relief, mean and maximum slope, circularity, compactness and Strahler order) were grouped by Ward's hierarchical agglomerative method[47]. No internal validation index identified a single optimal number of clusters: the morphometric space forms a near-continuum whose only strongly separated division isolates the large high-relief catchments from the remaining small coastal basins, and the silhouette[48], elbow, Calinski–Harabasz and Davies–Bouldin criteria disagree across k = 2–8 (Extended Data Fig. 4). Therefore, we adopted a four-cluster partition as the most parsimonious grouping that yields geomorphologically distinct and interpretable catchment types (Fig. 2), a choice reflecting interpretability and management relevance rather than internal-index optimality. Principal component analysis was used for visualisation.

Principal components analysis. To visualise the morphometric space and the cluster structure, the same seven standardised variables were subjected to principal component analysis[49] on the correlation matrix (i.e. computed from the z-scored variables). The analysis served for display only and did not enter the clustering. The first two components, retained for the biplot (Fig. 2B), together explained 71.6% of the total variance (42.1% and 29.5%): the first axis is a joint size–relief gradient, on which area, relief, slope and Strahler order load together, and the second captures basin shape, contrasting the circularity ratio with the Gravelius compactness coefficient. Catchments are shown as component scores coloured by cluster, with the variables as loading vectors (Fig. 2B).

Flood-risk and hazard analysis. Official recognition was taken from the SNCZI register of Areas with Potential Significant Flood Risk (APSFR) (https://www.miteco.gob.es/es/cartografia-y-sig/ide/descargas/agua/descargas_agua_snczi.html). Catchments were intersected with the SNCZI modelled flood extents for the T_{50}, T_{100} and T_{500} return periods in an equal-area projection (ETRS89-LAEA, EPSG:3035); coverage is the percentage of catchment area within each extent. ARPSIs are delineated in the preliminary flood risk assessment (EPRI) required by RD 903/2010, which identifies areas of potential significant risk from documented historical events, mainly those compiled in the national catalogue of historical floods (https://www.miteco.gob.es/en/agua/temas/gestion-de-los-riesgos-de-inundacion/cnih.html), and from pre-existing hydraulic studies; hazard mapping then follows the SNCZI methodological guide (https://www.miteco.gob.es/en/agua/temas/gestion-de-los-riesgos-de-inundacion/snczi/guia-metodologica-determinacion-zonas-inundables.html), which starts from the watercourses of the official hydrographic network. A stream absent from that network, and without a documented flood record, therefore falls outside the selection frame before any hazard assessment takes place.

A composite morphometric hazard proxy combined min–max-normalised mean slope (0.4), relief (0.3) and compactness (0.3), summarising morphometric flashiness rather than modelled hydraulic hazard; the mapped–unmapped comparison is insensitive to this weighting (equal weights and a data-driven first principal component of the seven morphometric variables give the same non-significant result, Mann–Whitney $p = 0.08$ and 0.16, and the three indices correlate $\rho = 0.79$–0.99).

As an independent check on hydrological hazard, peak discharges for the 100-year design storm were estimated for all catchments with the modified rational method (Témez; Instrucción 5.2-IC) from design rainfall, area, Hack main-channel length and slope, an imperviousness- and rainfall-dependent runoff coefficient and threshold, and the Témez time of concentration and uniformity coefficient; identical assumptions were applied to all catchments, so the screening supports group comparison rather than site-specific design; catchment-specific 2D hydraulic modelling would be required for design-level assessment of individual streams, which lies outside the scope of a regional inventory.

Extreme precipitation. Return-period quantiles of annual maximum daily precipitation (50-, 100- and 500-year) were downloaded from a gridded extreme-precipitation dataset (≈2.5 km resolution; https://retornolluvias.csic.es/), developed and validated for the Spanish mainland[50] and subsequently extended to the Balearic Islands, with quantiles calculated from precipitation series spanning 1961–2024. Each catchment was assigned the value (mm) of the grid cell at its centroid; for the few coastal catchments whose centroid fell on a sea cell, the nearest valid land cell was used (maximum displacement 1.8 km, below the grid spacing). The resulting quantiles increase monotonically with return period for every catchment. Precipitation quantiles were related to latitude, to the modelled flooded fraction of each catchment, and to catchment imperviousness, slope and income by Spearman rank correlation.

Catchment imperviousness. Soil sealing in each catchment was derived from the Copernicus Land Monitoring Service High-Resolution Layer Imperviousness Density (IMD) for 2021[23], a 100-m raster giving the percentage of impervious surface per cell (https://land.copernicus.eu/en/products/high-resolution-layer-imperviousness/imperviousness-density-2021; ETRS89-LAEA, EPSG:3035). Catchment boundaries were reprojected to the same system and zonal statistics computed over all intersecting tiles, excluding non-valid cells (values > 100). For each catchment we report the mean imperviousness, the maximum, and the fraction of catchment area exceeding 30% sealing. Because the mean is taken over the entire catchment, it indexes overall catchment urbanisation rather than the sealing of the buried reach itself, and is diluted in large headwater catchments whose urbanised reaches lie near the outlet; the proportion of heavily sealed area (> 30%) and the maximum are therefore more sensitive to localised burial. Imperviousness was compared between burial types and between recognised and unrecognised

catchments by two-sided Mann–Whitney U test, and related to morphometry, income and latitude by Spearman rank correlation.

Socioeconomic analysis. Catchment boundaries were spatially intersected with the 2021 national census-section cartography (https://www.ine.es/dyngs/DAB/index.htm?cid=1389); each section was assigned to the catchment of largest overlap and inherited its APSFR status. Per-section net income (ADRH 2021) and demographic indicators (2021 Census population, mean age, share aged ≥65) were available for all 190 sections (https://www.ine.es/censos2021/) and compared between recognised and unrecognised catchments by Mann–Whitney U test, and aggregated to the catchment level weighting by section population. Because census sections are nested within catchments and inherit their APSFR status, sections are not independent observations. The mapped–unmapped income contrast was therefore also tested at the catchment level with a cluster permutation test, in which APSFR status was randomly reassigned among the 45 catchments containing at least one section (5,000 permutations) and the section-level rank-biserial correlation recomputed each time. A cluster bootstrap, resampling whole catchments with replacement within each group (10,000 resamples), provided a 95% confidence interval that accounts for this nesting. Population-weighted income statistics describe the residents of the sections overlying each group of catchments; because sections are larger than the buried corridor, these figures describe the population of the catchments rather than of the culverted reach itself. The catchment-level comparison of population-weighted income is reported for completeness in Supplementary Table 1 and, with 17 and 28 catchments, has a statistical power of 0.11 for the observed effect (Cohen's d = 0.23). Exposed population per catchment was obtained by summing the population of its assigned census sections; the population density shown in Fig. 1B–D derives from the 2021 European census population grid (100 m resolution; Eurostat/GISCO, https://ec.europa.eu/eurostat/web/gisco/geodata/population-distribution/population-grids), reprojected to ETRS89-LAEA (EPSG:3035).

Statistics. Pairwise associations were quantified with the Spearman rank correlation; two-group comparisons with the two-sided Mann–Whitney U test. Significance was assessed at $p < 0.05$; asterisks denote $*p < 0.05$, $**p < 0.01$ and $***p < 0.001$. Effect sizes for two-group comparisons are reported as the rank-biserial correlation ($r = 2U/n_1n_2 - 1$, U being the statistic of the first group), quoted as absolute values with the direction of each contrast stated in the text, and with 95% confidence intervals from 5,000 bootstrap resamples. Statistical power was computed only for the catchment-level income comparison (Supplementary Table 1), for a two-sided two-sample test at $\alpha = 0.05$ from the non-central t distribution; because power functions are conventionally parameterised in standardised mean differences, the observed effect is there expressed as Cohen's d, which is used for this purpose alone. Analyses were performed in Python (SciPy, scikit-learn).

Centre values reported are medians unless stated; n denotes the number of catchments or census sections as indicated.

Data availability. The data analysed in this study derive from publicly available sources: official flood-hazard mapping (Areas of Potential Significant Flood Risk and modelled 50-, 100- and 500-year flood extents) from the Spanish National Cartographic System of Flood-Prone Zones (SNCZI, MITECO; https://www.miteco.gob.es); section-level income and demographic data from the Spanish National Statistics Institute (ADRH 2021 and 2021 Census, INE; https://www.ine.es); the 5-m PNOA digital terrain model from the National Geographic Institute (CNIG; https://centrodedescargas.cnig.es); the 2021 European census population grid from Eurostat/GISCO (https://ec.europa.eu/eurostat/web/gisco/geodata/population-distribution/population-grids); soil-sealing data from the Copernicus Land Monitoring Service (HRL Imperviousness Density 2021, EEA); and extreme-precipitation return-period data from the CSIC extraordinary-precipitation database (https://retornolluvias.csic.es/), used under the Open Database License. The derived per-catchment and census-section datasets that support the findings of this study are available in a public repository (https://doi.org/10.5281/zenodo.22807591).

Code availability. The Python code used for the morphometric, statistical, imperviousness and extreme-precipitation analyses is available, together with the derived datasets, in the same public repository (https://doi.org/10.5281/zenodo.22807591). Catchment delineation and spatial analyses were performed in QGIS and SAGA.

Acknowledgements. We thank A. Zamora for his assistance during the early stages of data collection.

Funding. This work was partially carried out within the LocAll4Flood project, co-funded by the European Union through the Interreg Euro-MED Programme.

Author contributions. C.G., J.L.-L. and R.J.B. conceived and designed the study. C.G., A.O.-M. and J.L.-L. compiled the ghost-river inventory and delineated the catchments. J.L.-L., E.M.-T. and A.O.-M. performed the morphometric, statistical, imperviousness and extreme-precipitation analyses. J.L.-L. and S.V.-M. carried out the socioeconomic and flood-risk analyses. J.L.-L. produced the figures. C.G. and J.L.-L. drafted the manuscript. All authors discussed the results, edited the manuscript and approved the final version.

Competing interests. The authors declare no competing interests.

References

1. Chin, A. O'Dowd, A. P. & Gregory, K. J. Urbanization and River Channels. In Treatise on Geomorphology (Academic Press, 2013) https://doi.org/10.1016/B978-0-12-374739-6.00266-9.

2. Elmore, A. J. & Kaushal, S. S. Disappearing headwaters: patterns of stream burial due to urbanization. *Front. Ecol. Environ.* **6**, 308–312 (2008).

3. Leopold, L.B. Hydrology for urban land planning - A guidebook on the hydrologic effects of urban land use: U.S. Geological Survey Circular 554 (1968) https://doi.org/10.3133/cir554.

4. Napieralski, J. et al. Urban stream deserts as a consequence of excess stream burial in urban watersheds. *Ann. Assoc. Am. Geogr.* **105**, 649–664 (2015).

5. Napieralski, J.A. & Welsh, E.S. A century of stream burial in Michigan (USA) cities. J. Maps, 1–5. (2016)

6. Weitzell, R. E. Kaushal, S. S. Lynch, L. M. Guinn, S. M. & Elmore, A. J. Extent of Stream Burial and Relationships to Watershed Area, Topography, and Impervious Surface Area. Water, 8(11), 538. (2016). https://doi.org/10.3390/w8110538

7. Meyer, J.L.; Paul, M.J.; Taulbee, W.K. Stream ecosystem function in urbanizing landscapes. *J. N. Am. Benthol. Soc.* 2005, **24**, 602–612 (2005)

8. Walsh, C J. et al. The urban stream syndrome: current knowledge and the search for a cure. *J. N. Am. Benthol. Soc.* **24(3)**, 706–723 (2005) doi:10.1899/04-028.1

9. Pinkham, R. *Daylighting: New Life for Buried Streams* (Rocky Mountain Institute, 2000).

10. Buchholz, T. & Younos, T. *Urban Stream Daylighting: Case Study Evaluations* (Virginia Water Resources Research Center, 2007).

11. Wild, T. C., Bernet, J. F., Westling, E. L. & Lerner, D. N. Deculverting: reviewing the evidence on the 'daylighting' and restoration of culverted rivers. *Water Environ. J.* **25**, 412–421 (2011).

12. Kang, C. D. & Cervero, R. From elevated freeway to urban greenway: land value impacts of the CGC project in Seoul, Korea. *Urban Stud.* **46**, 2771–2794 (2009). https://doi.org/10.1177/0042098009345166

13. Calvo-Sancho, C. Díaz-Fernández, J. González-Alemán, J.J. et al. Human-induced climate change amplification on storm dynamics in Valencia's 2024 catastrophic flash flood. *Nat Commun* **17**, 1492 (2026). https://doi.org/10.1038/s41467-026-68929-9

14. Llasat, M. C., Marcos, R., Turco, M., Gilabert, J. & Llasat-Botija, M. Trends in flash flood events versus convective precipitation in the Mediterranean region: the case of Catalonia. *J. Hydrol.* **541**, 24–37 (2016).

15. Tramblay, Y. & Somot, S. Future evolution of extreme precipitation in the Mediterranean. *Clim. Change* **151**, 289–302 (2018).

16. Zittis, G., Bruggeman, A. & Lelieveld, J. Revisiting future extreme precipitation trends in the Mediterranean. *Weather Clim. Extrem.* **34**, 100380 (2021). https://doi.org/10.1016/j.wace.2021.100380

17. Forgrave, R., Elliott, E. M. & Bain, D. J. Event scale hydrograph responses highlight impacts of widespread stream burial and urban infrastructure failures. *Hydrol. Process.* **36**, e14584 (2022). https://doi.org/10.1002/hyp.14584

18. Priest, S. J. et al. The European Union approach to flood risk management and improving societal resilience: lessons from the implementation of the Floods Directive in six European countries. *Ecology and Society* **21**(4) (2016).

19. Paul, M.J. & Meyer, J.L. Streams in the Urban Landscape. *Annual Review Ecology, Evolution, and Systematics* **32**, 333-365 (2001). https://doi.org/10.1146/annurev.ecolsys.32.081501.114040
20. Chin, A. Urban transformation of river landscapes in a global context. *Geomorphology* **79**, 460–487 (2006). 10.1016/j.geomorph.2006.06.033
21. Andreadis, K.M. et al. Urbanizing the floodplain: global changes of imperviousness in flood-prone areas. *Environ. Res. Lett.* **17** 104024 (2022) DOI 10.1088/1748-9326/ac9197
22. Rubiera Morollón, F., González Marroquin, V. M., & Pérez Rivero, J. L. Urban sprawl in Spain: differences among cities and causes. *European Planning Studies* **24**(1), 207–226 (2016). https://doi.org/10.1080/09654313.2015.1080230
23. European Union, Copernicus Land Monitoring Service. Imperviousness Density 2021 (raster 100 m), Europe, 3-yearly. European Environment Agency (EEA) https://land.copernicus.eu/en/products/high-resolution-layer-imperviousness/imperviousness-density-2021 (2025).
24. Fallowfield, L. & Motta, D. The permanent flood risk of culverts and the impact of increasing debris blockage. *Journal of Flood Risk Management* **17**(4), e13021. (2024).https://doi.org/10.1111/jfr3.13021
25. Truhlar, A. M., Marjerison, R. D., Gold, D. F., Watkins, L., Archibald, J. A., Lung, M. E., Meyer, A., & Walter, M. T. Rapid remote assessment of culvert flooding risk. Journal of *Sustainable Water in the Built Environment* **6**(2) (2020). https://doi.org/10.1061/JSWBAY.0000900
26. Fornés, J. M., López-Gunn, E., & Villarroya, F. Water in Spain: paradigm changes in water policy. *Hydrological Sciences Journal* **66**(7), 1113–1123 (2021). https://doi.org/10.1080/02626667.2021.1918697
27. Smith, N. Uneven Development: Nature, Capital and the Production of Space. (University of Georgia Press, 2008)
28. Gaume, E. et al. A compilation of data on European flash floods. *J. Hydrol.* **367**, 70–78 (2009).
29. Marchi, L., Borga, M., Preciso, E. & Gaume, E. Characterisation of selected extreme flash floods in Europe and implications for flood risk management. *J. Hydrol.* **394**, 118–133 (2010).
30. Dunne, T. & Leopold, L.B. Water in environmental planning. (San Francisco: W. H. Freeman, 1978)
31. Martín-Vide, J. P. Restoration of an urban river in Barcelona, Spain. *Environ. Eng. Policy* **2**, 113–119 (1999). https://doi.org/10.1007/s100220000030
32. Portugués Mollà, I. Management of the Turia River in Valencia (Spain): The Recent History of an Unfinished Metamorphosis. In: Farguell Pérez, J., Santasusagna Riu, A. (eds) Urban and Metropolitan Rivers. The Urban Book Series (2024). Springer, Cham. https://doi.org/10.1007/978-3-031-62641-8_9
33. European Cort of Auditors. Floods Directive: progress in assessing risks, while planning and implementation need to improve. Special Report nº 25. (2018) https://op.europa.eu/webpub/eca/special-reports/floods-directive-25-2018/en/

34. Real Decreto 903/2010, de 9 de julio, de evaluación y gestión de riesgos de inundación. *Boletín Oficial del Estado* **171**, 61954–61967 (2010). https://www.boe.es/eli/es/rd/2010/07/09/903
35. Bubeck, P., Botzen, W. J. W. & Aerts, J. C. J. H. A review of risk perceptions and other factors that influence flood mitigation behavior. *Risk Anal.* **32**, 1481–1495 (2012).
36. Kasperson, R. E. & Kasperson, J. X. The social amplification and attenuation of risk. *Ann. Am. Acad. Pol. Soc. Sci.* **545**, 95–105 (1996). https://doi.org/10.1177/0002716296545001010
37. Walker, G. & Burningham, K. Flood risk, vulnerability and environmental justice: evidence and evaluation of inequality in a UK context. *Crit. Soc. Policy* **31**, 216–240 (2011). https://doi.org/10.1177/0261018310396149
38. Tate, E., Rahman, M. A., Emrich, C. T. & Sampson, C. C. Flood exposure and social vulnerability in the United States. *Nat. Hazards* **106**, 435–457 (2021). https://doi.org/10.1007/s11069-020-04470-2
39. Cutter, S. L., Boruff, B. J. & Shirley, W. L. Social vulnerability to environmental hazards. *Soc. Sci. Q.* **84**, 242–261 (2003).
40. Schlosberg, D. *Defining Environmental Justice: Theories, Movements, and Nature* (Oxford Univ. Press, 2007).
41. Star, S. L. The ethnography of infrastructure. *Am. Behav. Sci.* **43**, 377–391 (1999). https://doi.org/10.1177/00027649921955326
42. Nixon, R. *Slow Violence and the Environmentalism of the Poor* (Harvard Univ. Press, 2011).
43. Scott, J. C. *Seeing Like a State: How Certain Schemes to Improve the Human Condition Have Failed* (Yale Univ. Press, 1998).
44. O'Callaghan, J. F. & Mark, D. M. The extraction of drainage networks from digital elevation data. *Comput. Vis. Graph. Image Process.* **28**, 323–344 (1984).
45. Conrad, O. et al. System for Automated Geoscientific Analyses (SAGA) v. 2.1.4. *Geosci. Model Dev.* **8**, 1991–2007 (2015).
46. Strahler, A. N. Quantitative analysis of watershed geomorphology. *Trans. Am. Geophys. Union* **38**, 913–920 (1957).
47. Ward, J. H. Hierarchical grouping to optimize an objective function. *J. Am. Stat. Assoc.* **58**, 236–244 (1963).
48. Rousseeuw, P. J. Silhouettes: a graphical aid to the interpretation and validation of cluster analysis. *J. Comput. Appl. Math.* **20**, 53–65 (1987).
49. Jolliffe, I. T. & Cadima, J. Principal component analysis: a review and recent developments. *Phil. Trans. R. Soc. A* **374**, 20150202 (2016).
50. González-Hidalgo, J. C., Beguería, S., Peña-Angulo, D. & Trullenque-Blanco, V. Catalogue and analysis of extraordinary precipitation events in the Spanish mainland, 1916–2022. *Int. J. Climatol.* e8785 (2025).

Supplementary Files

This is a list of supplementary files associated with this preprint. Click to download.

- SupplementaryInformation.docx
- ExtendedData.docx